A PROBABILISTIC APPROACH TO LANDSLIDE SUSCEPTIBILITY MAPPING USING MULTI-TEMPORAL AIRBORNE LIDAR DATA

Omar E. Mora, PhD Candidate
Charles K. Toth, Research Professor
Dorota A. Grejner-Brzezinska, Professor
The Ohio State University
Columbus, OH 43210
mora.30@osu.edu

M. Gabriela Lenzano, Research Assistant
Geomatics Department, National Council of Scientific and Technological Research (CONICET)
Mendoza, Argentina

ABSTRACT

A probabilistic approach is proposed to aid landslide susceptibility mapping. The objective of the proposed approach is to identify and predict areas that may develop into landslides and quantify the growth of existing landslides with high probability. Change detection was applied to repeat airborne Light Detection and Ranging (LiDAR) surveys acquired in December of 2008 and April of 2012. The study area was along the transportation corridor of Muskingum State Route 666 in Zanesville, Ohio, an area characterized by high vegetation densities, stream and river channeling, and some residential development. In the investigation, changes between LiDAR-derived Digital Elevation Models (DEM) were computed by analyzing, cell-by-cell, the vertical differences and, consequently, generating a DEM of Difference (DoD) map. Then, a parametric z-test was used to evaluate probabilistically if single-cell differences were real as compared to noise. Next, a non-parametric signed rank test was used to assess local neighborhoods and compute the probability that the median of the samples surpassed a desired threshold. Finally, high-probability neighborhoods (clusters) comprised of a minimum area and desired probabilities were mapped as "landslide susceptible". The initial results, obtained by comparison to a reference landslide map, were as expected, indicating that segments of the mapped landslides experienced changes, while others did not. It was also observed that some unmapped areas also experienced changes, indicating that they may be developing landslides. This study demonstrates that the monitoring of existing and identification of newly developing landslides is feasible from multi-temporal airborne LiDAR data.

Key words: Multi-temporal, LiDAR, landslide, change detection, probabilistic

INTRODUCTION

Landslides are difficult to predict and cause economic, human, and environmental damage worldwide (Glenn et al., 2006). They have a broad range of geological processes that cause the downward movement of mass over spatial and temporal scales (McKean and Roering, 2004). In addition, their effects have a strong dependability on their spatial pattern of incident angle, rate of recurrence, and amount of movement (McKean and Roering, 2004). Their hazards are well-understood, yet current methods of identifying and assessing their conditions are not time- and/or cost-effective and normally consist only of conventional geotechnical techniques. Current methods typically are based on field inspection, aerial photograph interpretation, and old contour map analysis (Booth et al., 2009). However, these methods have limitations that reduce the accuracy and completeness necessary to map landslides with high probability, consequently reducing their dependability (Booth et al., 2009; Galli et al., 2008). Additionally, many sites are not easily accessed for field inspections. Highly vegetated areas make difficulties for both on-site inspections and aerial photographic interpretation. Moreover, historical contour maps do not have the resolution necessary to map small landslides in highly vegetated areas where conventional remote-sensing techniques cannot penetrate the land cover (Van Den Eeckhaut et al., 2005; Booth et al., 2009; James et al., 2011). For these reasons, traditional mapping techniques are not optimal and a new approach to landslide susceptibility mapping is necessary.

Remote-sensing technology has seen phenomenal advances in the past decade. One of the major improvements

has been the increased spatial resolution of Light Detection and Ranging (LiDAR) technology. In the early advances in LiDAR technology, coarse nominal point spacing (> 10 meters) were available. Improvement of this technology has allowed for higher spatial resolutions (< 1 meter). This increase in spatial resolution provides mapping opportunities at remarkable scales. LiDAR technology provides the accuracy necessary to map surface models precisely (Shan and Toth, 2008; Jaboyedoff et al., 2010). Furthermore, it has become more accessible and affordable. Landslide susceptibility mapping is faced with many challenges that LiDAR technology may help overcome. These include, for example, spatial resolution, broad terrain coverage, and the accuracy necessary to map precise surface models. A LiDAR technology capable of overcoming the aforementioned challenges is airborne LiDAR. It has the ability to penetrate vegetation and map areas up to thousands of square kilometers (Shan and Toth, 2008; Guzzetti et al., 2012). In addition, it is capable of providing sub-meter level spatial resolutions at high accuracy levels.

In the early 1990s, Lane et al. (1994) introduced repeat topographic surveys to produce DEM of Difference (DoD) maps by utilizing rigorous analytical photogrammetry with ground survey. The ability to observe surface deformation from change detection on DEMs presented a new opportunity to identify, predict and quantify surface deformations that may develop into landslides. The elevation changes detected provide locations, processes, and rates of change (James et al., 2011). Assuming that real surface deformations can be distinguished from measurement uncertainties, this makes DoD maps highly attractive, as they provide a means to monitor temporal changes (Wheaton et al., 2010a; Wheaton et al., 2010b; DeLong et al., 2012). In order to monitor temporal changes properly it is additionally required that Digital Elevation Model (DEM) generation and multi-temporal registration be performed appropriately (DeLong et al., 2012).

Multi-temporal remote-sensing techniques have been used to measure surface processes by performing change detection to map erosion, deposition, and volumetric change (e.g., Lane et al., 1994; Wheaton et al., 2010a; Wheaton et al., 2010b; DeLong et al., 2012). Topographic change detection over large areas in landslide terrains has consisted of such methods (or a combination thereof) as field observation, traditional surveying, aerial photograph interpretation, global positioning system (GPS), and airborne LiDAR (Kelsey, 1978; Baum et al., 1998; Malet et al., 2002; Glenn et al., 2006; Mackey et al., 2009; Coe et al., 2009; Mackey and Roering, 2011). While these methods provide landslide kinematics and mechanics, none of them provide sub-meter horizontal and vertical maps of topographic change (DeLong et al., 2012).

This study presents results of a proposed probabilistic approach for landslide susceptibility mapping utilizing multi-temporal airborne LiDAR-derived DEMs. The approach analyzes cell-by-cell vertical differences observed between two LiDAR-derived DEMs. The changes observed are then evaluated probabilistically by employing the parametric z-test to assess if the observed changes are real or noise. Next, local neighborhoods are analyzed probabilistically utilizing the non-parametric signed rank test to evaluate if the median of the observed probabilities surpass a confidence level. Finally, high-probability neighborhoods (clusters) comprised of a minimum area and desired probabilities are mapped as landslide susceptible. To assess the performance of the proposed landslide susceptibility mapping technique, a comparison is performed to quantify the surface deformation of new and existing landslides with respect to the provided landslide inventory map.

METHODOLOGY

A probabilistic approach to landslide susceptibility mapping provides a new form to identify and predict areas that may develop into landslides and to quantify the growth of existing landslides with a high degree of probability. DoD maps provide temporal changes, but determining the source of the change (e.g., erosion, deposition, subsidence, uplift) is complex (James et al., 2011). A workflow diagram of the proposed probabilistic approach to landslide susceptibility mapping utilizing multi-temporal airborne LiDAR data is shown in Figure 1.

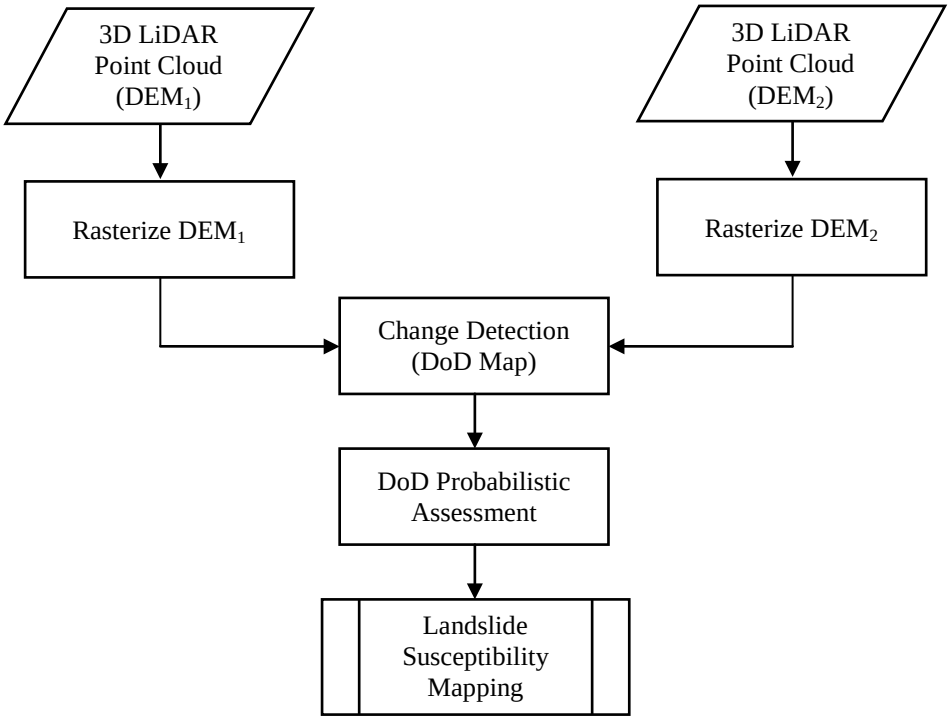

Figure 1. Workflow diagram for the proposed probabilistic approach to landslide susceptibility mapping utilizing multi-temporal airborne LiDAR data.

Characterizing DEM Uncertainty

The uncertainty in a DEM can be separated into horizontal and vertical components. The positional error in the horizontal component, being larger in magnitude than the vertical component for LiDAR technology, has an effect on the observed vertical differences, especially in sloped areas. LiDAR is rarely characterized by horizontal errors, therefore only the vertical component is analyzed, though the horizontal error does have an impact on vertical components. Furthermore, our interest is to analyze the vertical changes in the DoD map, therefore the vertical uncertainties are of high interest. The variable δz can be associated to the actual vertical component (Z_{Actual}) as follows:

$$Z_{Actual} = Z_{DEM} + \delta z \quad (1)$$

where Z_{Actual} is the true vertical component, Z_{DEM} is the observed vertical component, and δz is the vertical positional error. Many approximations, ranging from manufacturer instrument precision to error budget analysis, have been proposed to evaluate δz (Lichti et al., 2005). Nonetheless, there are many components that affect δz other than manufacturer instrument precision. These include: measurement errors, spatial sampling, and interpolation methods (Wheaton et al., 2010a). Furthermore, error budget analysis requires data collection and testing techniques that go beyond conventional survey methods, which are dominated by the collection of ground-control-utilizing GPS to evaluate the data quality in order to estimate δz. Statistically characterizing the precise magnitude of δz (including distribution type, RMS, and standard deviation) requires more information than can be provided in the topographic data (Wheaton et al., 2010a).

Propagation of DEM Uncertainty into DoD

Assuming that the uncertainties in the DEMs are normally distributed and uncorrelated, individual errors in the DEMs were propagated by Brasington et al. (2003) into the DoD as follows:

$$\delta u_{DoD} = \sqrt{(\delta z_2)^2 + (\delta z_1)^2} \quad (2)$$

where δu_{DoD} is the propagated error in the DoD, and δz_2 and δz_1 are the individual errors in DEM_2 and DEM_1, respectively. The assumption made is that the errors in each cell are independent and random. Moreover, the error can be computed to be consistent throughout the DoD if δz_2 and δz_1 do not exhibit patterns that are coherent and predictable in spatial variability (Wheaton et al., 2010a), which is our assumption.

Assessing DoD Uncertainty

A common approach to the evaluation of DEM uncertainties incorporates a minimum level of detection threshold ($_{min}$LoD) to distinguish real surface deformation from noise (Fuller et al., 2003). Observed elevation changes below this threshold are typically ignored, and those above are treated as real. However, there have been questions as whether the propagated error used to estimate the $_{min}$LoD also should be used in changes over a threshold. For example, if the $_{min}$LoD is 15 cm and the observed change was 50 cm, should the change be 50 cm or 50 cm ± 15 cm. In our approach, we consider the observed change to be 50 cm (no threshold-corrected data) and the propagated uncertainties (δu_{DoD}) will be used to characterize the DoD map. The importance of the propagated uncertainty (δu_{DoD}) is that it helps define the probability that the observed changes in the DoD are real.

Parametric Z-Test

The parametric z-test was used to evaluate the probability that the surface deformation experienced was real when compared to uncertainties propagated in the DoD. The parametric approach assumes that the propagated uncertainties can be approximated by a normal distribution. This test is performed on single-cell observations given a mean (μ) and a standard deviation (δu_{DoD}) of the propagated uncertainties in the DoD. Working with single-cell observations, we would like to evaluate the probability (P_z) that the observed change was real. In order to do so, we need to evaluate the following:

$$\sigma_z = \frac{\Delta_{DoD} - \mu}{\delta u_{DoD}} \quad (3)$$

where Δ_{DoD} is the observed difference in the DoD (DEM_2 - DEM_1), and σ_Z is the standard deviation of the observed difference compared to the uncertainties propagated in the DoD. The probability (P_z) of the observed Δ_{DoD} representing real surface deformation is then evaluated using the computed σ_Z and the assumption that the propagated uncertainties are normally distributed. Given σ_Z and the assumption of normality, the probability can be computed for the observed differences lying symmetrically within ($-\sigma_Z$, σ_Z).

Non-Parametric Signed Rank Test (Wilcoxon)

A probabilistic signed rank test is proposed to evaluate local neighborhoods of probabilities generated from the z-test. The non-parametric signed rank test developed by Wilcoxon (1945) makes no assumption about the underlying distribution, thus making our predictions more robust in the form that the distribution is not dependent of any parent distribution nor of its parameters. The signed rank test evaluates the null hypothesis (H_0: $\theta \geq M$) that the observations in the local neighborhood ($w \times w$ *cells*) come from a continuous distribution with a median greater than M (Wolfe and Hollander, 1999), where θ is the treatment effect (in our case the observed probabilities from the z-test). For this assessment, we computed P where P is the probability that the null hypothesis is true. The left-tail test is performed at a given level of significance (α) to test the following:

$$H_0: \theta \geq M \text{ vs. } H_1: \theta < M \quad (4)$$

Throughout this paper, the 95% level of significance (α) is used as a threshold for this technique. For more details on the non-parametric signed rank test see Wilcoxon (1945) and Wolfe and Hollander (1999).

Probabilistic Landslide Susceptibility Mapping

The final step of the proposed approach to landslide susceptibility mapping is evaluating local neighborhoods (clusters) generated from the signed rank test. In this step, clusters having a probability greater than a desired threshold are retained. In addition, a threshold is set for the minimum area to be considered as susceptible to landslides. Finally, all clusters meeting both constraints and thresholds are considered landslide susceptible with a high degree of probability.

STUDY AREA

The study area selected was along the transportation corridor of State Route (SR) 666 in Zanesville, Ohio, located in north-central Muskingum County along the east side of the Muskingum River. The study area begins at the intersection of SR-60 within the City of Zanesville just north of Interstate 70 (I-70) and south of the Muskingum River at mile marker (MM) 0.00, and ends at the intersection with SR-208 east of the Village of Dresden at MM 14.34. The area is characterized by high vegetation densities, stream and river channeling, and some residential development. The study area was chosen due to the availability of an airborne LiDAR-derived DEM, a detailed landslide inventory map, and its prolonged history of slope instabilities, especially in areas where the river is close to the roadway. In 2004 and 2005, Muskingum County was declared a National Disaster Area due to extensive flooding along major and minor streams. Figure 2 presents an overview map of the study area.

Figure 2. Study area along SR-666 (purple line), north of Zanesville, OH.

DATA

LiDAR data acquired in the winter of 2008 and spring of 2012, with point densities of 3 and 5 pts/m^2, respectively, was used in this research. The extent of the project coverage is 23 km along SR-666 having a varying width of 75 to 180 meters. The vertical accuracy of the points was assessed after the LiDAR was adjusted to the hard-surface control. Then, the vertical accuracy for both hard- and soft-surface controls was compared to the adjusted LiDAR. The vertical accuracy of the points was assessed by the root mean square error (RMSE), which was 9 cm for soft surfaces and 5 cm for hard surfaces. Additionally, the vertical accuracy was evaluated by the standard deviation, which was 6 cm and 5 cm for soft and hard surfaces, respectively. The bare-earth, filtered from the LiDAR data, was subsequently used for this investigation. The LiDAR point cloud was bare-earth filtered, and then interpolated to a spatial resolution of 50 cm using kriging, after evaluating the nominal point spacing to be 45 cm. The preprocessing of the bare-earth LiDAR data, including conversion to a regular grid, was done via LAStools (Isenburg, 2012) and ArcGIS software. All sequential processing was performed in MATLAB. The results of the processing steps were integrated into the project Geographical Information System (GIS) database.

For the project area, a geohazard inventory and evaluation of mass movement affecting the transportation network was completed in 2006 by the Ohio Department of Transportation (ODOT) Office of Geotechnical Engineering. This provided important information about the general locations of landslides affecting the road prism. An updated landslide inventory map was compiled by a team of experts from Kent State University and The Ohio State University through contour map analysis, geohazard inventory evaluation and on-site validation in the summer of 2012. The updated landslide inventory was used for the investigation. In Figure 3, A and B illustrate two typical landslides affecting the road prism. The importance of the inventory map is that it provides a reference against which we can evaluate the performance of our proposed approach. A limitation found in the inventory map is that it provides only the extents of the mapped landslides and does not offer additional information about the rate of change experienced. In our study, the mapped landslides provided in the inventory range from 200 m^2 to 27,000 m^2 in area.

(A) MM 7.3 (B) MM 1.47

Figure 3. (A) Examples of rotational slides, affecting the embankment near SR-666 mile markers 7.3 (A) and 1.47 (B), respectively; extents outlined in red.

RESULTS AND ANALYSIS

Raw Observations

The first step in evaluating the proposed approach to probabilistic landslide susceptibility mapping is to assess the cell-by-cell differences computed from the multi-temporal airborne LiDAR data. These differences are the raw changes observed; they are illustrated in Figure 4A. The maximum uplift and subsidence observed within the area illustrated were 170 and 247 cm, respectively. Furthermore, the estimated mean and standard deviation were 1 and 18 cm, respectively, for the observed changes within the entire study area. In addition, a hillshade DEM is shown in Figure 4B to complement the raw observations and portray the relief depiction of the chosen study area. The hillshade map demonstrates areas with high topographic variability compared to its neighboring regions. This may be an indication that surface deformation has occurred over time for these particular regions. The regions displaying this behavior are outlined in red and blue in Figure 4B. The region outlined in blue is of particular interest as it was an area mapped as landslide susceptible in the inventory map. Therefore, close attention will be paid to this particular area in order to evaluate if the mapped landslide exhibits high-probability vertical changes over the time

span between the LiDAR surveys.

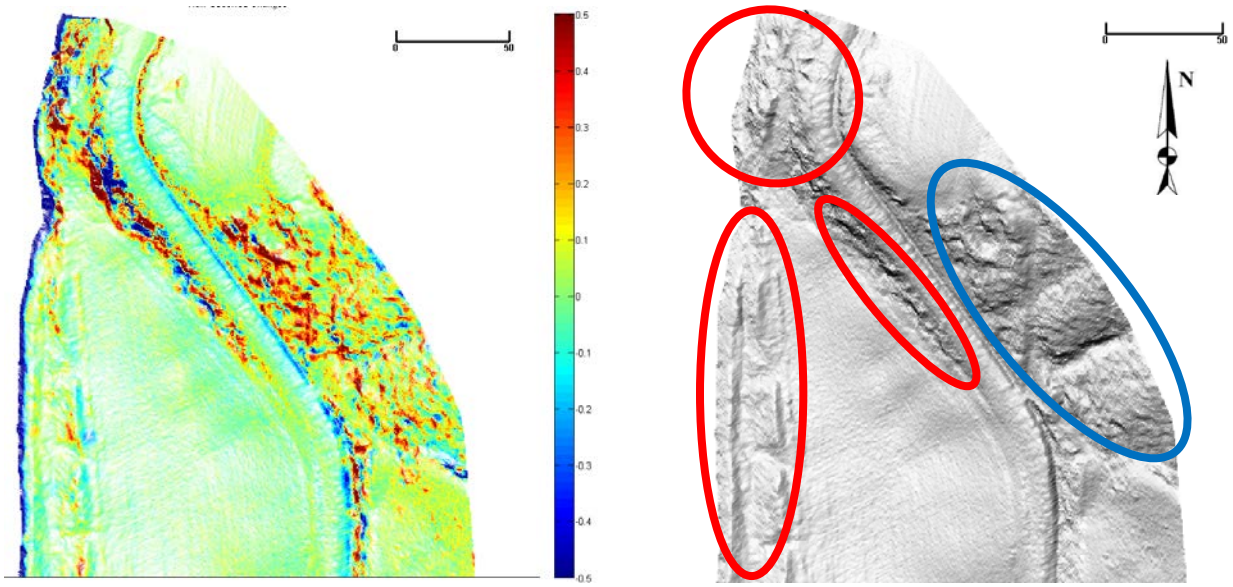

(A) (B)

Figure 4. The DoD map and the hillshade map are illustrated in (A), and (B), respectively. The scale bar for (A) and (B), and the legend in (A) are in meters. Regions experiencing high topographic variability are outlined in red and blue in (B). The region outlined in blue in (B) was an area mapped as a landslide in the inventory map.

The raw observations indicate that surface deformation has occurred for the areas displaying high topographic variability. These areas are outlined in red in Figure 4B, and include a mapped landslide outlined in blue. In addition, the raw observations illustrate that smoother topography experienced less change than those regions displaying higher topographic variability. McKean and Roering (2004) demonstrated that the surfaces of landslides are rougher than neighboring unfailed terrain. Our results support the fact that the amount of change expected is to be lower for unfailed, smooth topography, than for areas where active mass movement generates higher degrees of surface deformation. The mapped landslide region outline in blue appears to have experienced uplift, and this behavior is consistently displayed for this particular area. The remaining outlined regions outlined in red do not show a particular pattern, seeming to have experienced both subsidence and uplift in no particular order. Moreover, the west side of the study area is along the bank of the Muskingum River and, therefore, consistently displays subsidence/erosion along this particular area. This behavior is expected as the soil will erode over time into the river. Analysis of the DoD map illustrates that changes of various magnitudes were observed for this particular area. Consequently, the study area was ideal to test our proposed approach.

Probabilistic Landslide Susceptibility Mapping Approach

After evaluating the raw differences, the probability that each difference is real and not noise can be evaluated utilizing Equation (3). The probabilistic z-test generates a probability map as shown in Figure 5A. Given the mean and distribution of the uncertainties in the DEMs, with $\mu = 0$ cm, $\delta z_2 = 6$ cm, and $\delta z_1 = 6$ cm, the propagated uncertainties can be computed as illustrated in Equation (2). An advantage of the z-test is that it employs the raw vertical changes, and determines the probability for each observation, under the assumption that the propagated uncertainties can be approximated by a normal distribution.

The results for the parametric z-test complement the raw differences illustrated in Figure 4A, as expected. The raw differences having the highest amount of difference also have the highest probability of the changes being real, as they lie on the outer limits of the propagated uncertainty. One limitation of the probability map is that it does not differentiate between uplift and subsidence, but it can easily be compared to the DoD map to resolve this issue. Our interest is not to evaluate the amount of uplift or subsidence occurring over time, rather our interest is simply to identify neighborhoods that experience surface deformation with high probability. Therefore, the probability map in Figure 5A is sufficient for the first step of the proposed approach since it provides the probabilities for single observations. The mean, median and standard deviation of the probabilities shown are 0.46, 0.39 and 0.33, respectively.

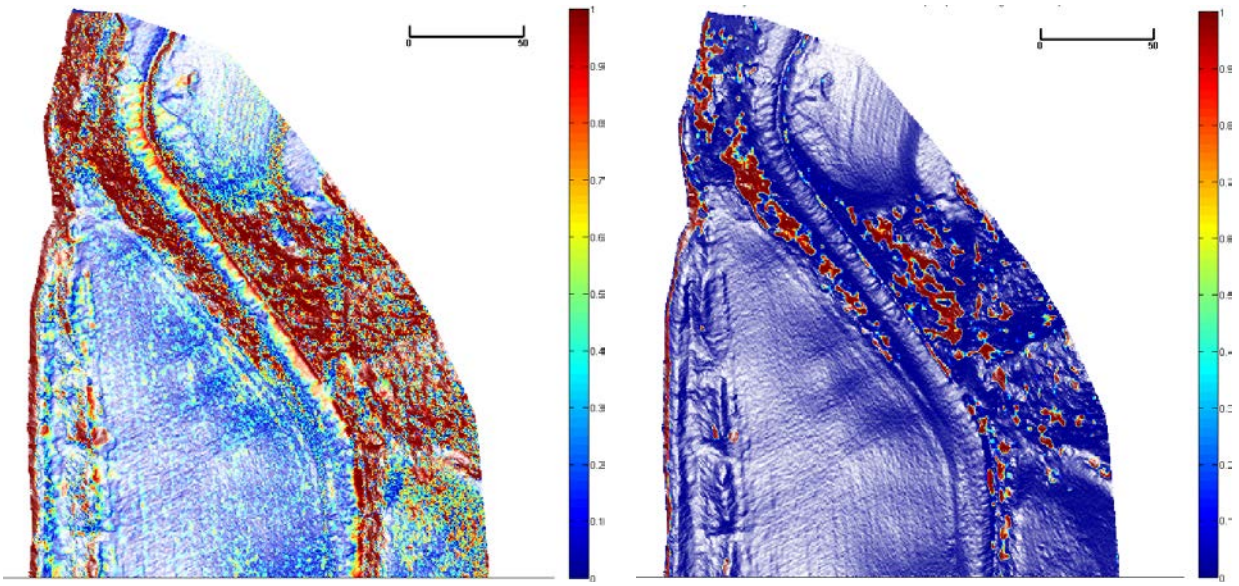

(A) (B)

Figure 5. Illustrated in (A) are the probabilities (z-test) that the surface deformations are real given μ = 0 cm and δu_{DoD} = 8 cm. Displayed in (B) are the probabilities computed from the signed rank test given a local neighborhood of *5* × *5* cells and *M* = 0.95. The scale bar for (A) and (B) is in meters. The legend for (A) and (B) is in units of probability.

A probabilistic, non-parametric signed ranked test (Wilcoxon, 1945) was subsequently used to analyze local neighborhoods. One advantage of the signed rank test is that is makes no assumption about the underlying distribution of the samples, and in our case we have no information about the distribution. Local neighborhoods of *5* × *5* cells are used to evaluate the central pixel in the window. The signed rank test evaluates the probability that the median of the samples in the neighborhood are greater than 0.95, therefore corresponding to the fact that the local neighborhood does indeed experience surface deformation with high probability. Illustrated in Figure 5B are the probabilities generated from the signed rank test.

Clusters of high-probability surface deformation are clearly depicted in Figure 5B, suggesting that these local areas do experience real surface deformation. In addition, the high-probability clusters coincide with the mapped landslide outlined in blue in Figure 4B. illustrating that this landslide area exhibits high-probability surface changes. Furthermore, it is noted that high-probability clusters are also observed along the western edge of the road, suggesting that these may be newly developing landslides and/or that the already mapped landslide (reference) has developed further. It is noted that the riverbanks are also mapped with high-probability clusters, suggesting that erosion is experienced in these regions. Finally, portions of the areas outlined in red in Figure 4B experiencing high topographic variability are shown to experience changes with high probability, therefore suggesting that topographic variability does correspond to landslide surface deformation, as expected.

The final step of the proposed probabilistic approach is to identify clusters generated from the signed rank test having an area greater than 25 m^2 and a probability of 0.90. Clusters meeting said constraints were mapped and the mean difference observed within the cluster was computed. Outlined in black in Figure 6 are these mapped clusters with their respective mean differences observed. The mapped landslides from our proposed algorithm coincide with the mapped landslide from the inventory map and those areas experiencing high topographic variability. In addition, it is observed that the mapped landslides closer to the riverbanks experience higher amounts of surface deformation compared to those more distant. Furthermore, the range between the mean differences observed between the mapped clusters is 31 – 83 cm, suggesting that not all regions experience the same amount of surface deformation.

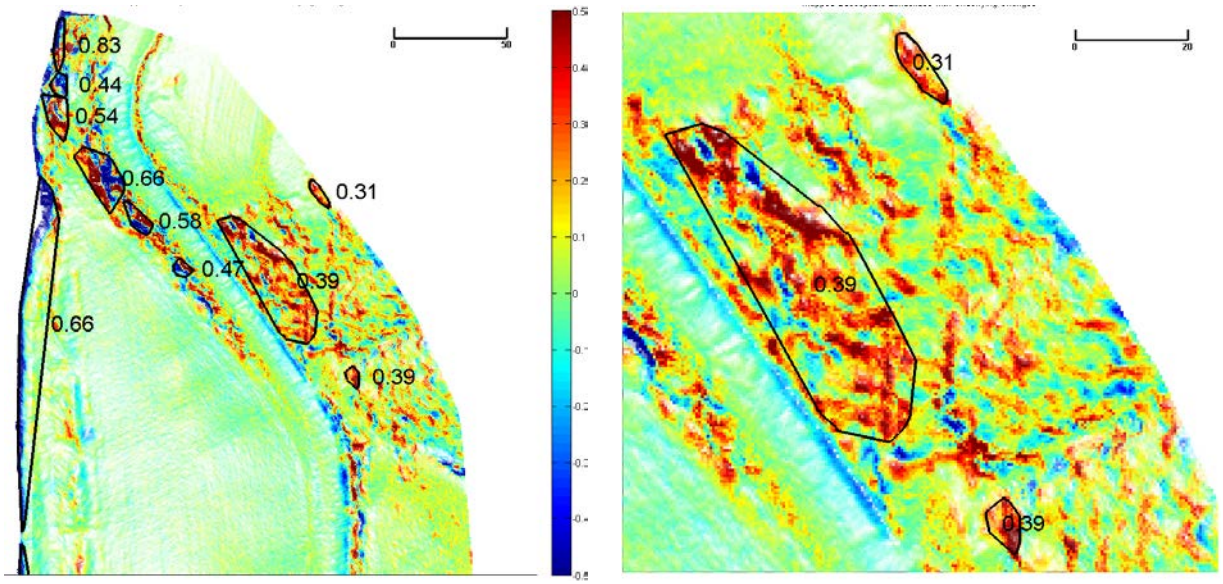

(A) (B)

Figure 6. Mapped landslides (outlined in black) utilizing proposed approach with underlying DoD map. The scale bar, legend and mean changes are in meters. (A) illustrates the entire area analyzed, while (B) illustrates in detail the areas mapped on the east side of the road.

CONCLUSIONS

This study has introduced a new landslide susceptibility mapping technique for quantifying changes with high probability from DoDs. The new mapping technique was applied to two LiDAR-derived DEMs collected 3.5 years apart coving part of SR-666 in Zanesville, Ohio. The developments from this study include the introduction of a probabilistic, non-parametric signed rank test to evaluate with high probability the changes exhibited in landslide-prone terrain. In addition, an evaluation is performed to quantify the surface deformation of new and existing landslides compared to the existing landslide inventory map.

The initial results from this study indicate that the monitoring of existing landslides and identification of newly developing landslides is feasible from multi-temporal airborne LiDAR data. Future work may include quantifying the amount of surface deformation experienced with high probability for each individual difference observed. Furthermore, areas depicting degrees of topographic variability higher than local neighboring terrain were mapped as being comprised of high-probability surface deformation, which corresponds to the idea that the surfaces of landslides are rougher than neighboring unfailed terrain.

Methods of change detection, especially DoD, are foreseen to be of interest as the availability and affordability of airborne LiDAR data continues to improve. Furthermore, advancements in airborne LiDAR will provide the higher spatial resolutions, terrain coverage and accuracy necessary to map surface models precisely, thus allowing for an increase in detectability of changes with respect to the spatial resolution. As uncertainties are reduced and DoD methods are improved, this will allow for higher confidence in landslide susceptibility analysis results. DoD will become important in landslide susceptibility mapping, where vertical changes reflect the spatial and temporal processes of mass movement. The limiting factor to study of the spatial and temporal processes of mass movement will be availability of high-quality data from which to build a DEM.

ACKNOWLEDGEMENTS

The authors wish to acknowledge the support of Kirk Beach from the Office of Geotechnical Engineering of the Ohio Department of Transportation. Also, the authors wish to acknowledge Dr. Jung-kuan Liu for his insight and feedback throughout this study.

REFERENCES

Baum, R.L., J. Messerich, and R.W. Fleming, 1998. Surface deformation as a guide to kinematics and three-dimensional shape of slow-moving, clay-rich landslides, Honolulu, Hawaii, *Environmental & Engineering Geoscience*, 4(3):283-306.

Booth, A.M., Josh J. Roering, and J.T. Perron, 2009. Automated landslide mapping using spectral analysis and high-resolution topographic data: Puget Sound lowlands, Washington, and Portland Hills, Oregon, *Geomorphology*, 109(3):132-147.

Brasington, J., J. Langham, and B**.** Rumsby, 2003. Methodological sensitivity of morphometric estimates of coarse fluvial sediment transport, *Geomorphology*, 53(3):299-316.

Coe, J.A., et al., 2009. Basal-topographic control of stationary ponds on a continuously moving landslide, *Earth Surface Processes and Landforms*, 34(2):264-279.

DeLong, S.B., et al., 2012. Multitemporal ALSM change detection, sediment delivery, and process mapping at an active earthflow, *Earth Surface Processes and Landforms*, 37(3):262-272.

Fuller, I.C., et al., 2003. Reach-scale sediment transfers: An evaluation of two morphological budgeting approaches, *Earth Surface Processes and Landforms*, 28(8):889-903.

Galli, M., et al., 2008. Comparing landslide inventory maps, *Geomorphology*, 94(3):268-289.

Glenn, N.F., et al., 2006. Analysis of LiDAR-derived topographic information for characterizing and differentiating landslide morphology and activity, *Geomorphology*, 73(1):131-148.

Guzzetti, F., et al., 2012. Landslide inventory maps: New tools for an old problem, *Earth-Science Reviews*, 112(1):42-66.

Hollander, M., D.A. Wolfe, and E. Chicken, 2013. *Nonparametric Statistical Methods*, Vol. 751, John Wiley & Sons.

Isenburg, M., LAStools - efficient tools for LiDAR processing. version 111216, http://lastools.org.

Jaboyedoff, M., et al., 2012. Use of LIDAR in landslide investigations: A review, *Natural hazards*, 61(1):5-28.

James, L.A., et al., 2012. Geomorphic change detection using historic maps and DEM differencing: The temporal dimension of geospatial analysis, *Geomorphology*, 137(1):181-198.

Kelsey, H.M., 1978. Earthflows in Franciscan melange, Van Duzen River basin, California, *Geology*, 6(6):361-364.

Lane, S.N., K.S. Richards, and J.H. Chandler, 1994. Developments in monitoring and modelling small-scale river bed topography, *Earth Surface Processes and Landforms*, 19(4):349-368.

Lichti, D.D., S.J. Gordon, and T. Tipdecho, 2005. Error models and propagation in directly georeferenced terrestrial laser scanner networks, *Journal of surveying engineering*, 131(4):135-142.

Mackey, B.H., J.J. Roering, and J.A. McKean, 2009. Long-term kinematics and sediment flux of an active earthflow, Eel River, California, *Geology*, 37(9):803-806.

Mackey, B.H., and J.J. Roering, 2011. Sediment yield, spatial characteristics, and the long-term evolution of active earthflows determined from airborne LiDAR and historical aerial photographs, Eel River, California, *Geological Society of America Bulletin*, 123(7-8):1560-1576.

Malet, J-P., O. Maquaire, and E. Calais, 2002. The use of Global Positioning System techniques for the continuous monitoring of landslides: Application to the Super-Sauze earthflow (Alpes-de-Haute-Provence, France), *Geomorphology*, 43(1):33-54.

McKean, J., and J. Roering, 2004. Objective landslide detection and surface morphology mapping using high-resolution airborne laser altimetry, *Geomorphology*, 57(3):331-351.

Shan, J., and C.K. Toth (editors), 2008. *Topographic Laser Ranging and Scanning: principles and processing*, CRC Press, Taylor and Francis Group.

Van Den Eeckhaut, M., et al., 2005. The effectiveness of hillshade maps and expert knowledge in mapping old deep-seated landslides, *Geomorphology*, 67(3):351-363.

Wheaton, J.M., et al. 2010a. Linking geomorphic changes to salmonid habitat at a scale relevant to fish, *River research and applications*, 26(4):469-486.

Wheaton, J.M., et al. 2010b. Accounting for uncertainty in DEMs from repeat topographic surveys: Improved sediment budgets, *Earth Surface Processes and Landforms*, 35(2):136-156.

Wilcoxon, F., 1945. Individual comparisons by ranking methods, *Biometrics*, 1(6):80-83.